relation is linear, as predicted by equation (3). This measurement is, to our knowledge, the first direct experimental verification of this important property—on which (among other things) the application of Luttinger-liquid theory to carbon nanotubes is based[13,14].

Fitting the measured dispersion relation to equation (3) yields the value of the Fermi velocity in nanotubes, $v_F = (8.2 \pm 0.7) \times 10^5\,m\,s^{-1}$. In a tight-binding description, v_F is related to the π–π overlap energy γ_0 by $v_F = 3^{1/2}\gamma_0 a_0/2\hbar$, where a_0 is the atomic lattice spacing. Our measurement thus corresponds to a value of $\gamma_0 = 2.6 \pm 0.2$ eV. For comparison, determinations of γ_0 based on the energies of van Hove singularities in STS and Raman spectroscopy measurements yield 2.5–2.9 and 2.6–3.0 eV, respectively[15]. Our determination of γ_0 based on a direct measurement of $E(k)$ performed near the Fermi level is therefore in agreement with those based on higher-energy structures. The fit also yields $E_0 - E_F = 0.34 \pm 0.03$ eV for the energy of the charge-neutrality point ($\delta k = 0$), in agreement with previous estimates[4,16].

Analysis of the variation of the energy-level spacing $\epsilon_{j+1} - \epsilon_j$ and of the energy-dependence of the coefficients $\phi_{j,n}$ of our wavefunctions reveals departures from recent theoretical predictions (A. A. Maarouf, N. R. Wilson and C. L. Kane, manuscript in preparation), suggesting that the electronic boundary conditions at the tube ends are energy-dependent. Interference effects have recently been invoked to explain transport measurements on SWNTs[17], but irregularities were observed that could also not be explained by assuming energy-independent boundary conditions. It is likely that harnessing these quantum-mechanical interference effects for practical devices will ultimately require the control of the atomic structure—and hence the electronic boundary conditions—at the nanotube ends. □

Received 4 June; accepted 13 July 2001.

1. Aviram, A. & Ratner, M. Molecular rectifiers. *Chem. Phys. Lett.* **29,** 277–283 (1974).
2. Joachim, C., Gimzewski, J. K. & Aviram, A. Electronics using hybrid-molecular and mono-molecular devices. *Nature* **408,** 541–548 (2000).
3. Bloch, F. Über die quantenmechanik der elektronen in kristallgittern. *Z. Phys.* **52,** 555–600 (1928).
4. Wildöer, J. W. G., Venema, L. C., Rinzler, A. G., Smalley, R. E. & Dekker, C. Electronic structure of atomically resolved carbon nanotubes. *Nature* **391,** 59–62 (1998).
5. Bronikowski, M. J., Willis, P. A., Colbert, D. T., Smith, K. A. & Smalley, R. E. Gas-phase production of carbon single-walled nanotubes from carbon monoxide via the HiPco process: a parametric study. *J. Vac. Sci. Technol. A* **19,** 1800–1805 (2001).
6. Venema, L. C. *et al.* Length control of individual carbon nanotubes by nanostructuring with a scanning tunneling microscope. *Appl. Phys. Lett.* **71,** 2629–2631 (1997).
7. Tersoff, J. & Hamann, D. R. Theory of the scanning tunneling microscope. *Phys. Rev. B* **31,** 805–813 (1985).
8. Rubio, A., Sánchez-Portal, D., Artocho, E., Ordejón, P. & Soler, J. M. Electronic states in a finite carbon nanotube: a one-dimensional quantum box. *Phys. Rev. Lett.* **82,** 3520–3523 (1999).
9. Kane, C. L. & Mele, E. J. Broken symmetries in scanning tunneling images of carbon nanotubes. *Phys. Rev. B* **59,** R1279–R12762 (1999).
10. Venema, L. C. *et al.* Imaging electron wave functions of quantized energy levels in carbon nanotubes. *Science* **283,** 52–55 (1999).
11. Crommie, M. F., Lutz, C. P. & Eigler, D. M. Imaging standing waves in a two-dimensional electron gas. *Nature* **363,** 524–527 (1993).
12. Hasegawa, Y. & Avouris, Ph. Direct observation of standing wave formation at surface steps using scanning tunneling spectroscopy. *Phys. Rev. Lett.* **71,** 1071–1074 (1993).
13. Egger, R. & Gogolin, A. O. Effective low-energy theory for correlated carbon nanotubes. *Phys. Rev. Lett.* **79,** 5082–5085 (1997).
14. Kane, C., Balents, L. & Fisher, M. P. A. Coulomb interactions and mesoscopic effects in carbon nanotubes. *Phys. Rev. Lett.* **79,** 5086–5089 (1997).
15. Dresselhaus, G. *et al.* in *Science and Application of Nanotubes* (eds Tománek, D. & Enbody, R.) 275–295 (Kluwer Academic/Plenum, New York, 2000).
16. Venema, L. C. *et al.* Spatially resolved scanning tunneling spectroscopy on single-walled carbon nanotubes. *Phys. Rev. B* **62,** 5238–5244 (2000).
17. Liang, W. *et al.* Fabry-Perot interference in a nanotube electron waveguide. *Nature* **411,** 665–669 (2001).

Acknowledgements

We thank C. L. Kane for discussions and for making theoretical results known to us before publication. This work was supported by NASA, the Dutch Foundation for Fundamental Research (FOM) and the European Union IST-FET program SATURN.

Correspondence and requests for materials should be addressed to S.L. (e-mail: lemay@mb.tn.tudelft.nl).

Observation of individual vortices trapped along columnar defects in high-temperature superconductors

A. Tonomura*†, H. Kasai*†, O. Kamimura*†, T. Matsuda*†, K. Harada*†, Y. Nakayama†‡, J. Shimoyama†‡, K. Kishio†‡, T. Hanaguri†§, K. Kitazawa†§, M. Sasase‖ & S. Okayasu‖

* *Advanced Research Laboratory, Hitachi Ltd, Hatoyama, Saitama 350-0395, Japan*
† *CREST, Japan Science and Technology Corporation (JST), Kawaguchi, Saitama 332-0012, Japan*
‡ *Department of Applied Chemistry, University of Tokyo, Tokyo 113-8656, Japan*
§ *Department of Advanced Materials Science, School of Frontier Sciences, University of Tokyo, Tokyo 113-0033, Japan*
‖ *Department of Material Science, Japan Atomic Energy Research Institute, Tokai, Naka-gun, Ibaraki 319-1195, Japan*

Many superconductors do not entirely expel magnetic flux—rather, magnetic flux can penetrate the superconducting state in the form of vortices. Moving vortices create resistance, so they must be 'pinned' to permit dissipationless current flow. This is a particularly important issue for the high-transition-temperature superconductors, in which the vortices move very easily[1]. Irradiation of superconducting samples by heavy ions produces columnar defects, which are considered[2] to be the optimal pinning traps when the orientation of the column coincides with that of the vortex line. Although columnar defect pinning has been investigated using macroscopic techniques[3,4], it has hitherto been impossible to resolve individual vortices intersecting with individual defects. Here we achieve the resolution required to image vortex lines and columnar defects in $Bi_2Sr_2CaCu_2O_{8+\delta}$ (Bi-2212) thin films, using a 1-MV field-emission electron microscope[5]. For our thin films, we find that the vortex lines at higher temperatures are trapped and oriented along tilted columnar defects, irrespective of the orientation of the applied magnetic field. At lower temperatures, however, vortex penetration always takes place perpendicular to the film plane, suggesting that intrinsic 'background' pinning in the material now dominates.

There are several methods of directly observing vortices, but none of them can determine the behaviour of individual vortex lines inside superconductors. This is because these methods detect vortices at the superconductor surfaces, even though an attempt has been made to obtain evidence of wandering vortex lines near material defects by using a two-sided Bitter decoration technique to detect the vortex positions on both sides of the film[6]. At present, the only methods which enable the observation of individual vortices and defects inside superconducting thin films are Lorentz microscopy[7] and interference microscopy[8], where the vortex magnetic fields are detected using a penetrating electron beam. However, owing to the low penetration power of the existing 300-kV field-emission electron beam, only a film thinner than the diameter of the vortex magnetic flux (that is, twice the magnetic penetration depth) has been observed. Vortex lines oriented in different directions cannot be distinguished in such a thin film, because the vortex magnetic fields inside it do not change very much.

To obtain clear images of vortices inside thicker films, we have developed a large electron microscope[5]. This 40-ton microscope has a 1-MV field-emission electron beam that has more than twice the penetration power of a 300-kV beam and also the highest brightness ($2 \times 10^{10}\,A\,cm^{-2}\,sr^{-1}$) ever attained. These features of the electron beam have allowed us not only to observe vortices in Bi-2212 films 400 nm thick with high contrast, but also to

distinguish between two vortex lines[9], one perpendicular to the film plane and the other trapped along a tilted columnar defect.

A schematic of the observation principle is shown in Fig. 1. Film samples were prepared by cleaving a single crystal of Bi-2212 (transition temperature $T_c = 85$ K) grown by the floating-zone method[10]. The films were then obliquely irradiated with parallel 240-MeV Au^{15+} ions (incidence angle $\theta_\phi = 70°$) as sparsely as 0.05 ions μm^{-2}, or with a matching magnetic field of 0.1 mT. We intentionally made the column density extremely sparse in our experiments so that we could use untrapped vortex lines perpendicular to the film plane as reference lines to unambiguously distinguish vortex lines trapped along tilted columns. A collimated electron beam was applied incident to the tilted film (tilting angle $\alpha = 30°$) and a magnetic field was applied in an arbitrary direction (incidence angle $\theta = (-70°) - (+70°)$) as shown in the schematic. We then observed the Lorentz images obtained by image-defocusing.

Examples of the observation results at $\theta_\phi = \theta = 70°$ are shown in Fig. 2. In the in-focus image (Fig. 2a), the projected images of tilted columnar defects are seen as short black lines. As the defocusing distance Δf increases, the column images first disappear completely by image-blurring. At larger Δf values, spots with bright-and-dark contrasting features appear instead, as shown in Fig. 2b. These spots appear because the phase change of the transmitted electron beam due to the vortex magnetic flux is transformed into the visible intensity variations by image-defocusing. They are Lorentz images of vortices.

There are two kinds of images in this Lorentz micrograph: circular spots and elongated spots with lower contrast. The elongated spots are indicated by the arrows in Fig. 2b. Image simulation[9] reveals that the circular images correspond to vortex lines penetrating the film perpendicularly to the film plane and that the elongated images correspond to vortex lines trapped along tilted columns. The image elongation direction is not necessarily the same as that of the tilted columns because of the effect of the inclination of the sample film, and the image contrast is weakened because of the spread of the magnetic flux distribution owing to the tilting of vortex lines from the c axis.

The vortex line direction inside a superconductor can be more precisely determined by comparing its Lorentz images taken while the sample is rotated around an axis normal to the film surface with the corresponding simulated images. A perpendicular vortex line does not change its direction with this rotation, but a tilted vortex line does, owing to the precession. In addition, a comparison of the two images in Fig. 2a and b reveals that columnar defects can be found at the exact centres of the elongated vortex images; this indicates that the elongated images actually represent vortex lines trapped along tilted columnar defects. Vortex lines oriented in different directions can thus be observed as different Lorentz images.

We then investigated whether vortex lines remained trapped along columnar defects even when the direction of the magnetic field or the sample temperature changed. First, we rotated the magnetic field from the column direction ($\theta = 70°$) to the film normal direction ($\theta = 0°$). In so doing, however, the elongated vortex images did not change at all, indicating that the vortex lines at columns remained trapped along them. Even when we further tilted the magnetic field direction until $\theta = -70°$, the vortex lines remained trapped. Lorentz micrographs at $\theta = 70°$ and $\theta = -70°$ are shown in Fig. 3a and b. The elongated images are indicated by the arrows.

We also found that the elongated images remained unchanged when we increased T from 35 K to T_c. However, when we gradually decreased T, we found to our surprise that the trapped vortices at columnar defects began to "stand up" perpendicularly to the film plane between 12 and 14 K. Figure 3c shows a Lorentz micrograph of the vortices at $\theta = -70°$ when T was 10 K. The elongated vortex images with weak contrast at 35 K (Fig. 3b) had changed to circular vortex images (Fig. 3c), the same as those surrounding untrapped perpendicular vortices.

We also found that this change was not reversible; there was hysteresis when the temperature was increased or decreased. That

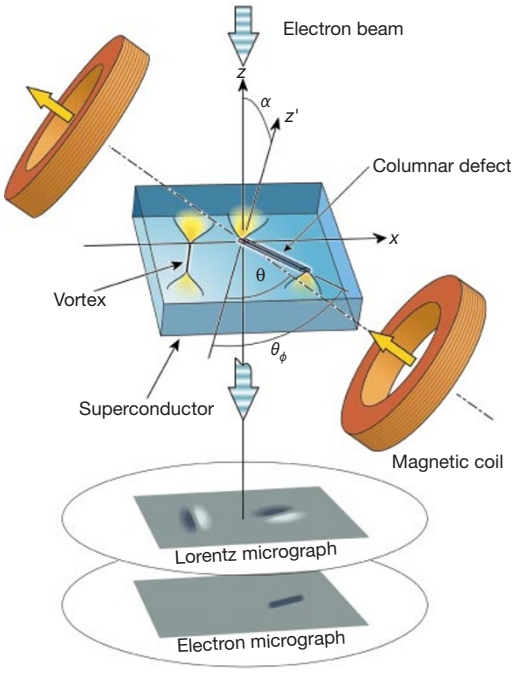

Figure 1 Lorentz microscopy of vortices in a superconducting Bi-2212 thin film with tilted columnar defects. The film is tilted at $\alpha = 30°$, α being the rotation angle around the x axis between the optical axis (z axis) and the film normal (z' axis). A magnetic field is applied to the film in the x–z' plane at an incidence angle of θ, thus producing vortices, whereas that of the column direction is θ_ϕ. An electron beam is vertically applied incident to the film, and the phase change of the transmitted beam that is due to the vortex magnetic flux inside the film is transformed into intensity variations as a Lorentz image by image-defocusing. The vortex images appear to be different for perpendicular and tilted vortex lines under appropriate defocusing distances.

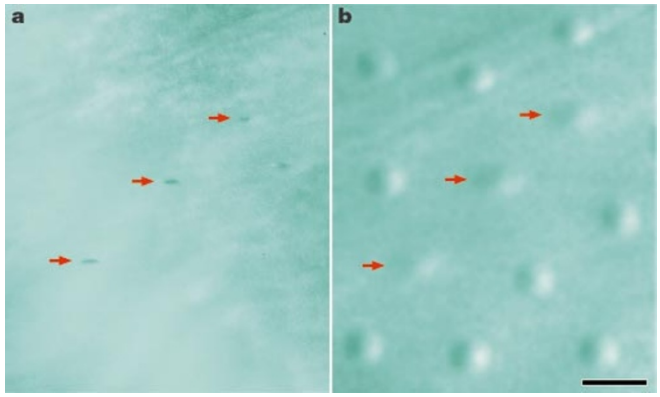

Figure 2 Vortices trapped and untrapped at columnar defects in Bi-2212 thin film ($H = 0.5$ mT, $\theta = \theta_\phi = 70°$). **a**, Electron micrograph. **b**, Lorentz micrograph ($\Delta f = 500$ mm, $T = 30$ K). Columnar defects can be seen as short black lines in the in-focus electron micrograph (**a**). When the micrograph is greatly defocused, the column images completely disappear and the vortex images appear instead as can be seen in the Lorentz micrograph (**b**): the images of the perpendicular vortex lines are circular, whereas those of the tilted vortex lines are elongated and have lower contrast. This was confirmed by image simulation and is illustrated in Fig. 1. It should be noted here that the elongated vortex images (indicated by the arrows in (**b**)) appear at the positions of the column images in (**a**). Owing to the low density of columnar defects, only some vortex lines are trapped along columnar defects; the others are untrapped and penetrate the film perpendicularly to the film plane. Scale bar, 2 μm.

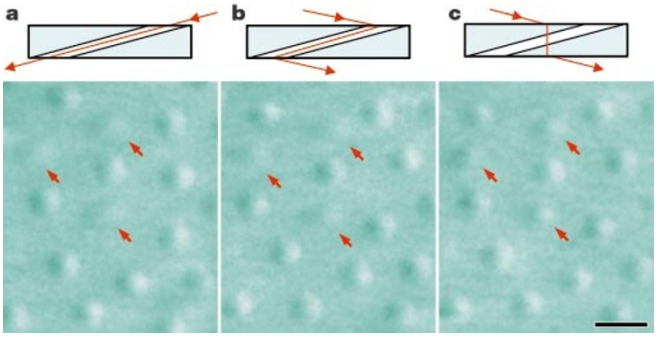

Figure 3 Lorentz micrographs showing vortex-line arrangements under various conditions. **a**, Magnetic field applied parallel to columns ($\theta = 70°$) at $T = 35$ K. **b**, Magnetic field applied in the direction of $\theta = -70°$ at $T = 35$ K. **c**, Magnetic field in the direction of $\theta = -70°$ at $T = 10$ K. The vortex lines trapped along columnar defects (in **a**) remained trapped even when the direction of the magnetic field was greatly tilted, as can be seen in **b** (indicated by the arrow). When T decreased, however, the vortex lines trapped along tilted columnar defects began to penetrate the film perpendicularly to the film plane at 12–14 K, even though the vortex lines were located at the positions of the columns, and therefore the vortex images became circular and their contrast became higher, as can be seen in **c**. Illustrations above each Lorentz micrograph indicate vortex-line arrangements. Scale bar, 2 μm. Video clips showing the behaviour of the vortices are available at http://www.hatoyama.hitachi.co.jp.

is, when T was increased, perpendicular vortex lines at 7 K began to tilt along columnar defects at 15–19 K, rather than at 12–14 K. The transition temperatures were rather scattered for the different vortex lines. For example, even at 7 K, we found vortex lines tilted at columns in very rare cases. This does not seem to originate from the different pinning forces of individual columns, because electron microscopy showed that column structures were fairly uniform in shape. Such tilting at 7 K may be due to the fact that very strongly pinned vortices are trapped simultaneously at multiple columns that gather by chance rather than at a single isolated column.

The observed behaviour of vortices can be interpreted by taking into consideration the temperature dependence of the pinning forces of columnar defects estimated from the observation of vortex movements. Above 25 K, changes in the magnetic field caused sparsely distributed vortices to hop from one columnar defect to another when a driving force was applied to them. Such a movement occurred regardless of the direction in which the magnetic field was applied. This can happen when columnar-defect pinning is dominant. These results are consistent with the previous observation that the vortex lines are firmly trapped even along greatly tilted columns irrespective of the direction of the applied magnetic field at $T > 19$ K.

When T was decreased below 25 K, the hopping movement gradually changed in such a manner that vortices intermittently stopped and migrated. This kind of movement can be interpreted to occur, because the background collective pinning due to more abundant smaller atomic-size defects of other types (for example, oxygen defects) is thought to increase relative to the columnar-defect pinning. The migration speed decreases at lower T; thus the migration is thought to be caused by thermally activated depinning of a vortex line from a large number of atomic-size defects one by one. The vortex lines, when stopped, were observed to be tilted along columns. When T was decreased below 12 K, however, the columnar-defect pinning became weaker relative to the background pinning, and trapped vortex lines at columnar defects were observed to stand up perpendicularly to the film plane. Around 7 K, all the vortices migrated or drifted uniformly when driven, as if the pinning force of columnar defects vanished and vortices were moving uniformly in a viscous medium. The pinning of columnar defects is almost completely hidden by the background pinning, although there were still some exceptional vortices that were strongly pinned, possibly at multiple defects.

In this way, direct observation microscopically elucidated the behaviour of vortices in Bi-2212 thin films. The isotropic pinning of vortices by columnar defects at low magnetic fields indirectly inferred by macroscopic magnetization measurements[3,11] can be explained microscopically by our experiments as follows: under our conditions of thin films, vortex lines are trapped along columns at temperatures above 19 K irrespective of the direction of the applied magnetic field; and at temperatures below 12 K vortex lines always penetrate the film perpendicularly to the film plane owing to the increased background pinning compared to the columnar-defect pinning and also because of the demagnetization effect of thin films. □

Received 27 March; accepted 4 June 2001.

1. Crabtree, G. W. & Nelson, D. R. Vortex physics in high-temperature superconductors. *Phys. Today* **50,** 38–45 (1997).
2. Civale, L. *et al.* Vortex confinement by columnar defects in $YBa_2Cu_3O_7$ crystals: Enhanced pinning at high fields and temperatures. *Phys. Rev. Lett.* **67,** 648–651 (1991).
3. Hardy, V. *et al.* Accommodation of vortices to tilted line defects in very high-T_c superconductors with various electronic anisotropies. *Phys. Rev. B* **54,** 656–664 (1996).
4. Schuster, Th. *et al.* Observation of in-plane anisotropy of vortex pinning by inclined columnar defects. *Phys. Rev. B* **50,** 9499–9502 (1994).
5. Kawasaki, T. *et al.* Fine crystal lattice fringes observed using a transmission electron microscope with 1 MeV coherent electron waves. *Appl. Phys. Lett.* **76,** 1342–1344 (2000).
6. Yao, Z., Yoon, S., Dai, H., Fan, S. & Lieber, C. M. Path of magnetic flux lines through high-T_c copper oxide superconductors. *Nature* **371,** 777–779 (1994).
7. Harada, K. *et al.* Real-time observation of vortex lattices in a superconductor by electron microscopy. *Nature* **360,** 51–53 (1992).
8. Tonomura, A. *Electron Holography* 2nd edn (Springer, Heidelberg, 1999).
9. Fanesi, S. *et al.* Influence of core misalignment and distortion on the Fresnel and holographic images of superconducting fluxons. *Phys. Rev. B* **59,** 1426–1431 (1999).
10. Kotaka, Y. *et al.* Doping state and transport anisotropy in Bi2212 single crystals. *Physica C* **235–240,** 1529–1530 (1994).
11. Klein, L., Yacoby, E. R., Yeshurun, Y., Konczykowski, M. & Kishio, K. Evidence for line vortices in $Bi_2Sr_2CaCu_2O_8$. *Phys. Rev. B* **48,** 3523–3525 (1993).

Acknowledgements

We are grateful to N. Hatano for his discussions on tilted columnar defects, and to G. Pozzi, M. Beleggia, N. Osakabe, T. Yoshida and J. Masuko for their simulations of Lorentz micrographs of tilted vortex lines. We also thank F. Nori for discussions and T. Akashi and I. Matsui for help with the experiments.

Correspondence and requests for materials should be addressed to A.T. (e-mail: tonomura@harl.hitachi.co.jp).

Vacancies in solids and the stability of surface morphology

K. F. McCarty, J. A. Nobel & N. C. Bartelt

Sandia National Laboratories, Livermore, California 94551-0969, USA

Determining how thermal vacancies are created and destroyed in solids is crucial for understanding many of their physical properties, such as solid-state diffusion. Surfaces are known to be good sources and sinks for bulk vacancies, but directly determining where the exchange between the surface and the bulk occurs is difficult. Here we show that vacancy generation (and annihilation) on the (110) surface of an ordered nickel–aluminium intermetallic alloy does not occur over the entire surface, but only near atomic step edges. This has been determined by oscillating the sample's temperature and observing in real time the response of the surface structure as a function of frequency (a version of Ångström's method of measuring thermal conductivity[1]) using low-energy electron microscopy. Although